Effect of Confinement on Cross-Sectional Performance of Steel-Concrete Composite Beams with Solid and Cellular Steel Sections

Author 1

- Pankaj R. Teware, Ph.D. student
- Department of Applied Mechanics, Visvesvaraya National Institute of Technology, Nagpur, India
- ORCID number: 0000-0001-6017-0210
- Email address: pankaj.teware@gmail.com

Author 2

- Dr. Ashish P. Khatri, Ph.D.
- Department of Applied Mechanics, Visvesvaraya National Institute of Technology, Nagpur, India
- ORCID number: 0000-0001-5178-8334
- Email address: ashishkhatri@apm.vnit.ac.in

Contact details of the corresponding author

Pankaj R. Teware, Ph.D. student

Email address: pankaj.teware@gmail.com

Effect of Confinement on Cross-Sectional Performance of Steel-Concrete Composite Beams with Solid and Cellular Steel Sections

Abstract

The purpose of this study is to compare the moment-curvature (M-ϕ) characteristics of a solid composite section (SCS) and a cellular composite beam section (CCS) under sagging moment. The strip method, which is based on fundamental mechanics principles that take into account linear strain variation across composite sections, was used to determine the M-ϕ. It is first developed for SCS for different parameters i.e., the grade of concrete, unconfined and confinement strength of concrete, and effective width of a concrete slab, and then, it is extended for CCS. The section of CCS has a 50% depth enhancement over the steel section of SCS. Full interaction between the steel beam and the slab up to the failure of a concrete slab is assumed in the analysis. According to the M-ϕ analysis, CCS enhances the ultimate moment capacity and the ultimate curvature for both unconfined and confined concrete. Concrete confinement for CCS was effective in boosting steel material utilization and resulting in higher curvature ductility before failure. The high concrete strength and wider effective flange width of the slab resulting in high ultimate moment capacity and ultimate curvature for SCS and CCS for unconfined and confined concrete.

Keywords: Solid composite sections, Cellular composite sections, Unconfined strength of concrete, Confined strength of concrete, Curvature ductility, Percentage utilization of material.

1 Introduction

The use of a composite beam in construction is often common due to several advantages of it. These composite beams are generally made up of steel-concrete materials in such a way that compression generated due to bending is resisted by concrete. The reduced height from floor to

floor due to the shallow depth of the composite beam is one of the advantages of such construction. Often, utility ducts are required to pass from one side to the other side of the composite beams. Passing these ducts through the web of a steel-rolled section of the composite beam result in the reduction of ultimate strength. The higher ultimate strength can be obtained by replacing the rolled steel section (parent section) with a cellular-steel beam having a higher depth as compared to the parent section. Thus, the use of a CCS results in strength enhancement and provision to pass the utility ducts simultaneously.

Achieving the higher ultimate moment (M_u) and ultimate curvature (ϕ_u) are the main prerequisites for composite beam sections. However, the current design codes[1,2] does not contain any guidelines for proportioning of composite beam sections. The utilization of composite action has been recognized as an effective way of enhancing structural performance[3]. A good design composite member can lead to significant savings in terms of section depth, material consumption, and overall cost, and lower environmental pollution and reduced energy consumption[4]. The effective composite action is formed at a sagging location. This location shows that each material is used to take advantage of its best attributes making the composite section efficient and economical[5]. It was proposed that under positive bending, the concrete slab provides buckling resistance to the top flange when it is subjected to compression[6], and the ductility of the steel allows for the achievement of high curvature[7]. The behaviour of the composite beam under negative moment was reversed, which results in the cracking in the slab and local buckling of the steel profile influencing the strength and ductility of the beams[8,9]. The ability of the steel flange or web to resist compression depends on its slenderness value, which is represented by its width-to-thickness ratio[10,11]. A simple rigid-plastic analysis of the section was carried out which shows that the positive moment capacity of a member can be increased by as much as 120% over the plain steel beam through composite action[12]. The analytical and

experimental work was carried out for predicting the ultimate strength and assuring the ductility of composite girders constructed using 250, 345, or 485 MPa grades of steel[13]. Their observation shows that a higher grade of steel enhanced the moment capacity but gives limited ductility for the composite section. Research paper[14] proposed that the failure of the composite beam with high-strength steel or concrete is brittle compared to beams with normal-strength steel and concrete. A method was presented for the ultimate strength analysis of composite beams with unreinforced rectangular web openings[15]. It was observed that the strength of a composite beam decreases with the increase of opening length and height. The location of the concentric web holes also plays an important role to resist the vertical load of the composite beam. An experimental study investigated the effect of concrete and steel strength, and concrete slab thickness on both buckling and the overall structural behaviour of composite beams under vertical load[3]. Results proposed a 25% increment in the ultimate load-carrying capacity of the composite castellated beam if web opening is provided after the negative moment region. To find the effect of castellation (hexagonal opening) on moment capacity and mid-span deflection of the composite beam, different castellation ratios were reported[16]. Their results depict the reduction in mid-span deflection and improvement in moment capacity with the increase of castellation ratio. The research paper [17] contains more details about the cellular composite beams. Concrete confinement also plays an important role in increasing the compression resistance of the concrete as per the stress-strain equation[18,19]. Ductility is a linear function of lateral confining pressure[20]. The confinement can be achieved by varying the spacing of the stirrups. The ultimate strength capacity and ductility of concrete beams increase as stirrup spacing decreases. As per[21,22] stirrups that enclose the concrete in the compression zone are more efficient than stirrups that run around the entire beam cross-section. To achieve satisfactory flexural strength and ductility, it was proposed that the stirrups were effectively placed in the bending zone[23,24].

Recent studies have concentrated more on the behaviour of web posts of the cellular composite beams, high-strength material, and buckling behaviour. It is still necessary to investigate how the composite beam cross-section performs under the influence of confined or unconfined strength of concrete, and structural steel with the cellular opening provided in the web. The present study particularly focused on exploring this behaviour in the form of the M-ϕ relationship of the CCS and SCS. A cellular beam section is defined as a steel beam with repeating concentric circular web openings. It is assumed to be made up of its parent rolled parallel flange section with a depth enhancement of 50%. They can be made from hot-rolled profiles by double-cutting and rewelding processes. The typical cross-section of the SCS and CCS sections is shown in **Figure 1(a,b),** respectively. For developing an M-Φ relationship, a full interaction without any slip between steel and concrete is assumed. The M-Φ characteristic of the composite beam was first developed for SCS and later for a CCS.

2 Algorithm of a developed program

The M-Φ analysis is performed based on the structural principles of mechanics. A flowchart of the developed program for M-Φ analysis which includes iterative calculations is shown in **Figure 2**. The variation of strain across the cross-section of SCS and CCS is considered linear as depicted in **Figure 3** (a-b). The analysis is first carried out for SCS for unconfined and confined concrete. The same procedure is modified and used for the CCS section by neglecting the contribution of web opening and assuming linear strain variation across the depth of the CCS.

The effectiveness of different cross-sections used for analysis is expressed in terms of percentage utilization of steel and concrete, respectively. Where percentage utilization of steel is the ratio of total tensile and compressive forces resisted by the steel section at the failure

stage to its capacity when all fibers are yielded and expressed in percentage. Similarly, percentage utilization of concrete is the ratio of the area of concrete under compression at the failure stage to the total area of concrete, expressed in percentage. These utilization ratios give an idea to effectively proportionate the cross-section area of steel and concrete for its maximum use and make the section economical and efficient.

3 Reliability of the developed program

Numerical simulation for CCS beams was done before the start of the parametric analysis. The finite element (FE) model for the developed program was created using the same numerical model setup as the numerical simulation, which was successful. The results of the developed program and FE model can be used for parametric analysis once the results have been verified.

3.1 Numerical Validation

The FE findings of cellular composite beams[25] were used to validate the present FE model through deflection response (d_{FEM}). The present FE model of the beam as shown in **Figure 4** is simply supported cellular composite beam subjected to a concentrated load at mid-span. The shear connectors embedded in solid concrete slab are used. For steel beam and concrete slab 4-noded shell elements and 4-noded multi-layered shell elements are used while for connectors 2-noded beam elements are used. The steel, concrete, and studs are characterized by linear elastic behaviour. The deflection response of the present FE model is validated with the literature FE results[25] which incorporate the additional deflection due to cellularity and with the proposed equation[25–27] for cellular composite beam. When compared to the present FE model, the deflection predicted by the equation is very consistent as per **Table 1**.

3.2 Validation of the developed program

To validate the developed program, solid 3D FE models of laterally restrained composite beams with a 600 mm b_{eff}, 200 mm slab thickness and a 6000 mm simply supported span were developed for different SCSs and CCSs as shown in **Figure 5**. These FE models of the beams are then subjected to uniform moment loading conditions to avoid any shear deformations in the beams. The parent NPB sections[28] has a depth (H) upsurge of 50% (H=1.5D) over its original depth (D) and the diameter of the provided web opening (d_0) is 67% of its enhanced depth (d_0 = 0.67H) is used. **Figure 6** and **Figure 7** shows the response of composite beams in terms of stress, and strain and **Figure 8** shows the M-φ relationship. The M-φ behaviour of composite beams as determined by the current FE model and developed program exhibits good agreement for all the considered beams, as depicted in **Figure 8**. All the behaviour shown is captured at the concrete's maximum allowable strain level of 0.0035, which is also the threshold for failure for composite beams. Using this validated FE model setup, the results of M-φ of an SCS and CCS, proposed by the developed program, are thus verified.

4 Parametric details

The aforementioned algorithm is used for analysing the M-Φ relationship of composite beams considering different parameters i.e., the strength of unconfined concrete, degree of confinement to the concrete, and effective flange width of the slab (b_{eff}). The details about these parameters are explained below.

4.1 Geometric characteristic

Hot rolled parallel flange NPB 350×250×79.18 section[28] is considered as a parent steel section for forming the composite beam. The cellular beam used is obtained from the parent section and is having a 50% depth enhancement without an increase in the total weight of the beam as

compared to the parent section. For avoiding the practical challenges of installing confining reinforcement to the concrete, a minimum 200mm depth of concrete slab is taken into consideration. The considered parameters along with their variation for analysis are shown in **Table 2**. The strength and ductility of the confined concrete depend on the arching action that occurs between the longitudinal bars and between transverse stirrups and links. Three different grades of concrete as listed in **Table 2** are considered[29] for determining the effect of concrete grade on confinement. The assumed reinforcement for providing confinement effect to the concrete slab is as per Table 3. The arrangement of assumed reinforcement is depicted in **Table 3.**

The steel and concrete grades as listed in **Table 2** are considered for analysis for examining their effect on composite beams. The stress-strain curve for concrete is developed based on the characteristic material strength of concrete[29]. The material characteristics used for the study do not include the corresponding material safety factors. However, size and shape correction factor of 0.85 was applied to the concrete used in the present study. The tensile strength of the concrete is also neglected. The bi-linearized material stress-strain characteristics without considering the material safety factor are used for structural steel beams both in tension and in compression.

4.1.1 Structural steel

Steel E250 grade [30], is considered for *M-Φ* analysis. The bi-linear stress-strain curve as shown in **Figure 9**, is used without considering the effect of strain hardening. Failure of the composite section is bound to occur when strain at the top fiber of the concrete slab reaches its ultimate strain value (ε_u) i.e. 0.0035. The corresponding value of ultimate strain in steel at the ultimate stage never reaches up to the strain hardening value, and hence strain hardening effect in steel

is neglected during analysis. Furthermore, it is assumed that the stress-strain characteristics of the steel are same in the compression and tension zones.

4.1.2 Unconfined concrete

In the present study, idealized stress-strain properties of unconfined concrete are considered for M25, M35, and M50 grades of concrete as shown in **Figure 10**. The maximum flexural stress in concrete is considered $0.67f'_c$ (f'_c is equivalent to f_{ck}) [29]. The obtained unconfined compressive strength for M25, M35, and M50 grades of concrete are 16.75 MPa, 23.45 MPa, and 33.50 MPa, respectively. This maximum stress in concrete is at a strain value of 0.002 and after this strain, stress is constant up to the ultimate strain of concrete. The behaviour of concrete at the yield and ultimate point for all considered grades is shown in **Figure 10**.

4.1.3 Confined concrete

The energy-balanced concept was used to predict the longitudinal compressive strain in the concrete corresponding to the first fracture of the transverse reinforcement by equating the strain energy capacity of the transverse reinforcement to the strain energy stored in the concrete as a result of the confinement[19]. In the present study, to find the confined strength of concrete a stress-strain model is being used[19]. The stress-strain model includes strength degradation characteristics after attaining the maximum confining strength along with an increase in strain value. Confinement of concrete by suitable arrangement of transverse reinforcement results in a slight increase in the flexural strength and a significant improvement in strain ductility of compressed concrete. The effectiveness of transverse reinforcement depends on the size of the confining core which intern depends on the spacing between longitudinal reinforcement. For this purpose, different assumed longitudinal reinforcement details and corresponding transverse reinforcement thereof for different flange width of the concrete slab is shown in **Figure 11**. The

proposed equation [19] is used to generate the confined stress-strain curve for the considered grade of concrete. The basic expression representing the proposed stress-strain relation is presented below.

For a monotonic loading, the longitudinal compressive stress f_c *is given by,*

$$f_c = \frac{f'_{cc} x r}{r - 1 + x^r} \quad \textbf{Eq. 1}$$

$$x = \frac{\varepsilon_c}{\varepsilon_{cc}} \quad \textbf{Eq. 2}$$

Where, ε_c = longitudinal compressive concrete strain.

$$\varepsilon_{cc} = \varepsilon_{co}\left[1 + 5\left(\frac{f'_{cc}}{f'_{co}} - 1\right)\right] \quad \textbf{Eq. 3}$$

Where, f'_{co} and ε_{co} = the unconfined concrete strength and corresponding strain (ε_{co} = 0.002 is used).

$$r = \frac{E_c}{E_c - E_{sec}} \quad \textbf{Eq. 4}$$

$$E_C = 5000\sqrt{f'_{co}} \quad \textbf{Eq. 5}$$

Where E_c is the tangent modulus of elasticity of concrete and

$$E_{sec} = \frac{f'_{cc}}{\varepsilon_{cc}} \quad \textbf{Eq. 6}$$

Where f'_{cc} = compressive strength of confined concrete.

$$f'_{cc} = f'_{co}\left(-1.254 + 2.254\sqrt{1 + \frac{7.94 f'_l}{f'_{co}}} - 2\frac{f'_l}{f'_{co}}\right) \quad \textbf{Eq. 7}$$

Where f'_l is the effective lateral confining stress on the concrete. With the help of this **Eq. 1** to **Eq. 7**, the confined compressive stress-strain characteristics for different grades of concrete and different effective widths are obtained and are presented in **Figure 12.**

From **Figure 12(a-c)** it is clear that a concrete slab with an effective flange width (b_{eff}) of 1000mm having 155mm center-to-center longitudinal bar spacing shows high confined strength and failure strain than others. This is due to the accessibility of high confining reinforcement available for the core concrete section. The strength and ductility of the section are increased as it is directly related to the amount of confinement available. Likewise, a lower grade of concrete has a higher percentage increase in strength and ultimate strain than a higher grade of concrete.

5 Behaviour of composite cross-section

All the possible combinations of the parameters mentioned in **Table 2** are used to determine the cross-sectional behaviour of SCS and CCS through the M-φ relationship. The analysis is divided into two different stages based on the strain value of cross-section i.e., elastic stage and inelastic stage. In the elastic stage, linear stress-strain behaviour is adopted for analysis while in the inelastic stage, the yielding of all fiber started from extreme fiber towards the neutral axis. The analysis is terminated when concrete material reaches its ultimate failure strain. Analysis results are compared based on the M_u, φ_u, and percentage utilization of steel and concrete material of the cross-section. All the composite sections show the initiation of yielding strain in the bottom flange of steel before the attainment of the 0.002 strain level at top fiber of concrete. For plotting of analysis results, a non-dimensional ratio between the moment capacity of section (M) to moment capacity at the yielding of section (M_y); and similarly for the curvature of section (ϕ/ϕ_y) is determined.

5.1 Effect of unconfined and confined strength of concrete

In this section, the composite section is analysed for the effect of unconfined and confined strength of different grades of concrete on SCS and CCS as shown in **Table 4**. From **Table 4**, it is observed that the M_u and φ_u are improved for CCS as compared to that of the SCS. As per observation, the composite beam with CCS exhibits improvements in M_u and φ_u of 18% and 12%, respectively, over SCS for a 600 mm wide concrete slab for unconfined M25 grade concrete. For the higher grade of concrete i.e., M50 grade, improvement in M_u and φ_u is 10% and 17%, respectively. It exemplifies how more ductile sections can be attained with a relatively low improvement at the moment with higher-grade concrete.

Table 4 makes it clear that CCS exhibits better ductility and moment resistance capacity when taking into account the confined strength of concrete for cross-sectional performance. The CCS exhibits a 17% and a 5% improvement in M_u and φ_u of the section, respectively, in comparison to SCS for a 600 mm wide concrete slab when confinement is provided to M25 grade concrete. When the confinement is through an M50 grade concrete, improvement in M_u and φ_u is 10% and 20%, as reported in **Table 4**. The M_u capacity of the CCS has improved less than the SCS under confinement, but the φ_u has improved significantly. The impact of the effective flange width of the concrete slab on the M_u and φ_u of the CCS and SCS is also noticeable. It demonstrates that increasing the b_{eff} improves the M_u and φ_u of the cross-section for both the confined and unconfined strengths of concrete.

5.2 *M-Φ* relationship for different grades of concrete

For determining the effect of the grade of concrete on the behaviour of the *M-Φ* relationship of SCS and CCS, the parameters mentioned in Table **2** and their combinations are examined. Analysis results obtained from the program are expressed in terms of a non-dimensional plot i.e., M_u/M_y, and φ_u/φ_y as depicted in **Figure 13(a,b)**. Besides that, the analysis is performed for

each of the slab widths listed in **Table 2** and the analysis outcomes of composite sections with slab widths of 1000 mm are only presented in this section.

For the SCS, the M_u/M_y after attainment of yielding of the cross-section is always higher than CCS for all the unconfined strength of concrete. CCS with M50 grade concrete results in a remarkable improvement in ϕ_u/ϕ_y after attaining yielding in cross-section as compared with SCS. Considering the confined strength of the concrete, the M_u/M_y and ϕ_u/ϕ_y ratio after yielding the cross-section are improved for SCS, and CCS as shown in **Figure 13(b)**. Confinement strength results in dynamic improvement of ϕ/ϕ_y in CCS when compared with SCS for a higher M50 grade of concrete.

5.2.1 Material utilization for different grades of concrete

The material utilization of the cross-section at the ultimate stage is influenced by the grade of concrete used for the composite beam. **Figure 14 (a)** illustrates the percentage of material used for beams having effective flange widths of 1000 mm and unconfined concrete strength. Similar material utilization under confined concrete strength is shown in **Figure 14 (b).** In **Figure 14 (a,b),** 'S' stands for an SCS, 'CL' stands for a CCS, 'st' stands for steel material, and 'c' stands for concrete material. Thus, for example; 'S-st' is the symbol used for representing the percentage utilization of steel material for SCS.

Figure 14 (a) demonstrates that as the grade of concrete increases, the percentage of concrete utilization decreases, while the percentage of steel utilization increases. Achieving higher percentage utilization of steel material is preferable on account of the higher cost associated with it, and also resulting in the required 'ductile failure' mode. The percentage utilization of concrete material is observed to be the least for the composite beam with a cellular steel section. The material utilization is greatly influenced by the effect of the confinement of

concrete. **Figure 14 (b)**, shows the steel cross-section is 100% utilized for all the grades of concrete while the utilization of concrete material goes on reducing. This shows that the increased strength due to confinement provided to the concrete results in a greater reduction of neutral axis depth (measured from the top fiber of the composite section) for a higher grade of concrete.

5.3 *M-Φ* relationship for different effective widths of the slab.

Although all the concrete grades listed in **Table 2** were taken into consideration, only the analysis results of composite sections with M25 grade concrete for various flange widths of the concrete slab are presented in this section for comparison purposes. **Figure 15 (a,b)**, shows the influence of the b_{eff} on the M_u/M_y and ϕ_u/ϕ_y ratios of the SCS and CCS cross-section.

For the SCS, the moment capacity ratio (M_u/M_y) after yielding of the cross-section is always higher than that of the CCS; for all the considered b_{eff} and concrete strengths. CCS with a higher b_{eff} results in a remarkable improvement of curvature ratio (ϕ_u/ϕ_y) after yielding in cross-section as compared with SCS for respective effective flange width of a concrete slab. Availability of a higher b_{eff} and confinement thereof results in a higher compressive force value which concrete can bear before failure. Therefore, for higher b_{eff}, M_u/M_y and ϕ_u/ϕ_y after yielding the cross-section are improved; for SCS, and CCS, respectively. Confinement to the concrete results in drastic improvement of ϕ_u/ϕ_y of CCS when compared with an SCS for higher b_{eff}.

5.3.1 Material utilization for different effective flange widths of slab

The percentage utilization of material for the composite beams with unconfined and confined strength of concrete is shown in **Figure 16 (a,b).** Moreover, these results are presented here for all considered composite beams having concrete of M25 grade with different b_{eff}. From **Figure 16 (a)**, the percentage utilization of concrete (for S-c versus CL-c) is reduced and for steel (for

S-st versus CL-st) it is increased for higher b_{eff}. It results in the least percentage utilization of concrete material for a CCS.

The higher b_{eff} gives a high confined strength to the concrete **Figure 16(b)**, shows the steel cross-section is almost 100% utilized for only higher b_{eff}, while utilization of concrete material goes on reducing for confined strength of concrete. This effect is enhanced for the CCS, and hence concrete utilization is minimum for a composite beam with a higher b_{eff} of a slab and cellular steel combination.

6 Conclusions

The strain compatibility-based moment-curvature program for SCS, and the CCS, is developed and verified with the FE model. The effect of cellularity and concrete confinement on the behaviour of solid and cellular composite beams was then observed through parametric analysis. Based on the analysis results presented herein the following conclusions are drawn.

- From the parametric study, it is observed that the behaviour of composite sections is enhanced under the effect of the confined strength of concrete and the use of cellular steel sections.

- In the case of unconfined SCS, the impact of increasing the effective width of the slab (b_{eff}) helps to improve the ultimate moment capacity (M_u) of composite sections. This impact is limited to certain higher grades of concrete. While in the case of ultimate curvature (ϕ_u), the impact of varying b_{eff} improves the ductile behaviour of composite sections.

- In the case of unconfined CCS, similar behaviour as shown by unconfined SCS was observed for ultimate moment capacity. However, when compared to unconfined SCS, an

improvement in ϕ_u has been seen as a result of increased effective slab width and escalating concrete grade.

- Concrete with confined strength impacts the ϕ_u of the SCS and CCS. For each considered increase in b_{eff} of confined CCS, a minimum of 1.5 times improvement in ϕ_u was obtained, while this improvement in the case of confined CCS is at least 2 times when compared with unconfined CCS.

- When it comes to CCS, the confinement that is given to the concrete allows for the most efficient use of the steel material and results in higher curvature ductility before failure than with unconfined SCS.

- The presence of a higher grade of concrete, and higher b_{eff}, whether it is unconfined or confined, results in better utilization of steel material for a CCS than that for an SCS.

Reference

1. IS 11384, Code of Practice for Composite Construction in Structural Steel and Concrete. BIS: 1985.
2. EN 1994-1-1, Eurocode 4: Design of Composite Steel and Concrete Structures- Part 1-1: General Rules and Rules for Buildings. CEN: *Bruxelles,* 2004.
3. Nethercot, D., *Composite construction* CRC Press, 2003.
4. Hauke, B., Economic application of composite beams with moderate high strength materials. In *5th European Conference on Steel and Composite Structures, Graz* 2008, pp. 3–5.
5. Nethercot, D. A., *Composite steel and concrete structural members: fundamental behaviour Eng Struct*, Fundamental Behaviour, Australia, 1996.
6. Shamass, R. and Cashell, K. A., Behaviour of Composite Beams Made Using High Strength Steel. *Structures*, 2017, **12**, 88–101.
7. Baskar, K. and Shanmugam, N. E., Steel-concrete composite plate girders subject to combined shear and bending. *J Constr Steel Res*, 2003, **59**, 531–557.

8. Vasdravellis, G., Uy, B., Tan, E. L., and Kirkland, B., Behaviour and design of composite beams subjected to negative bending and compression. *J Constr Steel Res*, 2012, **79**, 34–47.

9. Korkess, I. N., Yousifany, A. H., Abdul-majeed, Q., and Husain, H. M., Behavior of Composite Steel-Concrete Beam Subjected To Negative Bending. *Engineering and techonolgy*, 2009, **27**, 53–72.

10. IS 800, General Construction in Steel-Code of Practice. BIS: *New Delhi*, 2007.

11. Johnson, R. P., *Composite Structures of Steel and Concrete: beams, slabs, columns and frames for buildings* John Wiley & Sons, 2018.

12. Kirkland, B., Kim, P., Uy, B., and Vasdravellis, G., Moment-shear-axial force interaction in composite beams. *J Constr Steel Res*, 2015, **114**, 66–76.

13. Yakel, A. J. and Azizinamini, A., Improved moment strength prediction of composite steel plate girders in positive bending. *Journal of bridge engineering*, 2005, **10**, 28–38.

14. Zhao, H. and Yuan, Y., Experimental studies on composite beams with high-strength steel and concrete. *Steel and Composite Structures*, 2010, **10**, 373–383.

15. Ismail, R. E. S., Fahmy, A. S., and Tawfik, N. M., Ultimate Behavior of Composite Castellated Beams under Vertical Loads. *Int J Comput Appl*, 2014, **108**, 40–46.

16. Al-Zuhairi, A. H. A., Mansi, A. I., and Anbar-Iraq, B., Behavior of composite concrete castellated steel beams in flexur. In *1st International Conference on Recent Trends of Engineering Sciences Sustainability* 2017.

17. Ferreira, F. P. V., Martins, C. H., and de Nardin, S., Advances in composite beams with web openings and composite cellular beams. *J Constr Steel Res*, 2020, **172**.

18. Popovics, S., A numerical approach to the complete stress-strain curve of concrete. *Cem Concr Res*, 1973, **3**, 583–599.

19. Mander, J. B., Priestley, M. J. N., and Park, R., Theoretical Stress-Strain Model for Confined Concrete. *Journal of Structural Engineering*, 1988, **114**, 1804–1826.

20. Renić, T. and Kišiček, T., Ductility of concrete beams reinforced with frp rebars. *Buildings*, 2021, **11**.

21. Radnic, J., Markic, R., Harapin, A., and Matesan, D., Effect of confined concrete on compressive strength of RC beams. *Advances in concrete construction*, 2013, **1**, 215–225.

22. Bing, L., Park, R., and Tanaka, H., Stress-strain behavior of high-strength concrete confined by ultra-high- and normal-strength transverse reinforcements. *ACI Struct J*, 2001, **98**, 395–406.

23. Lokuge, W. P., Sanjayan, J. G., and Setunge, S., *Stress–Strain Model for Laterally Confined Concrete Journal of Materials in Civil Engineering*, 2005.

24. Jang, I.-Y., Park, H.-G., Kim, Y.-G., Kim, S.-S., and Kim, J.-H., Flexural Behavior of High-Strength Concrete Beams Confined with Stirrups in Pure Bending Zone. *Int J Concr Struct Mater*, 2009, **3**, 39–45.

25. Djebli, B., Elddine, D., and Abidelah, A., Additional and total deflection of composite symmetric cellular beams. *J Constr Steel Res*, 2019, **158**, 99–106.

26. Lawson, R. M., Lim, J., Hicks, S. J., and Simms, W. I., Design of composite asymmetric cellular beams and beams with large web openings. *J Constr Steel Res*, 2006, **62**, 614–629.

27. Chung, K. F. and Lawson, R. M., Simplified design of composite beams with large web openings to Eurocode 4. *J Constr Steel Res*, 2001, **57**, 135–164.

28. IS12778, Hot Rolled Parallel Flange Steel Sections for Beams, Columns and Bearing Piles — Dimensions and Section Properties. BIS: *New Delhi*, 2004.

29. IS 456, Plain and Reinforced Concrete-Code of Practice. BIS: *New Dehli*, 2000.

30. IS 2062, Indian Standard Hot Rolled Medium and High Tensile Structural Steel - Specification. BIS: 2011.

Table 1: Total deflection of CCS beam

Specimen; Reference	Deflection (mm)	d_{FEM}/d_i
d_{FEM}	18.15	1.00
d_1;[25]	18.00	0.99
d_2;[26]	18.00	0.99
d_3; [27]	16.70	0.92

Table 2: Considered parameters for SCS and CCS

Solid steel section	Cellular steel section	Slab geometry (mm)		Material grades (MPa)	
Details of NPB 350×250×79.18 (mm)		b_{eff}	t_s	Concrete	Steel
Depth (D) =340, Width of flange (b_f) = 250, Thickness of flange (t_f) = 14, Depth of web (d_w) = 312, Thickness of web (t_w) = 9	Enhanced depth (H) = 1.5×D, Diameter of web opening (D_o) =0.67×H, d_w = 482 mm	600, 800, and 1000	200	M25, M35, and M50	E250

Table 3: Details of reinforcement in the concrete slab of the composite section

b_{eff} (mm)	Assumed reinforcement on each face along the beam	Confining reinforcement of 8mm diameter @175 mm c/c
600	4 bars 12 mm in diameter	2 Nos. of two-legged stirrups
800	5 bars 12 mm in diameter	2 Nos. of two-legged stirrups + 2 Nos. of links
1000	7 bars 12 mm in diameter	3 Nos. of two-legged stirrups + 3 Nos. of links

Table 4: Effect of the strength of concrete

Grade of concrete	b_{eff} (mm)	SCS				CCS			
		Unconfined		Confined		Unconfined		Confined	
		M_u (kN-m)	ϕ_u	M_u (kN-m)	ϕ_u	M_u (kN-m)	ϕ_u	M_u (kN-m)	ϕ_u
M25	600	600	0.017	647	0.042	708	0.019	758	0.044
	800	657	0.019	719	0.058	762	0.021	808	0.069
	1000	708	0.021	763	0.098	809	0.023	839	0.116
M35	600	668	0.019	713	0.039	772	0.021	805	0.046
	800	737	0.022	765	0.063	824	0.025	840	0.075
	1000	775	0.027	797	0.100	848	0.032	864	0.12
M50	600	753	0.023	760	0.045	832	0.027	838	0.054
	800	792	0.031	797	0.069	852	0.037	864	0.083
	1000	815	0.038	823	0.106	876	0.045	882	0.127

Legends

SCS = Solid Composite Section

CCS = Cellular Composite Section

M-φ = Moment-curvature

M_u = Ultimate moment

ϕ_u = Ultimate curvature

b_{eff} = effective width of the slab

t_s = thickness of slab

B = width of flange

t_f = thickness of flange

t_w = thickness of web

D = Depth of solid steel section

D' = depth of SCS

H = the enhanced depth of I-section

H' = Depth of CCS

d_0 = depth of web opening

d_{wp} = depth of web post

NA = Neutral Axis

ε = Strain

ε_y = Yield strain

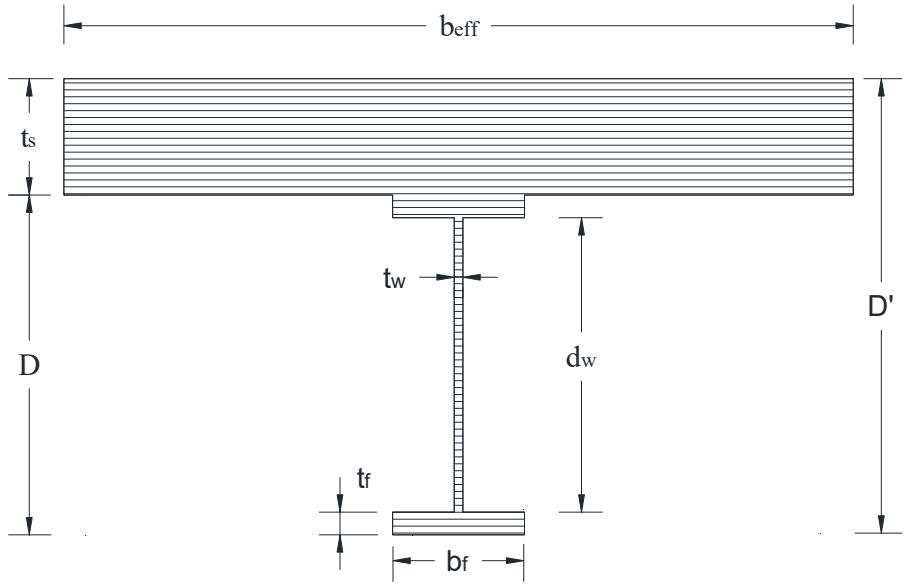

(a) SCS

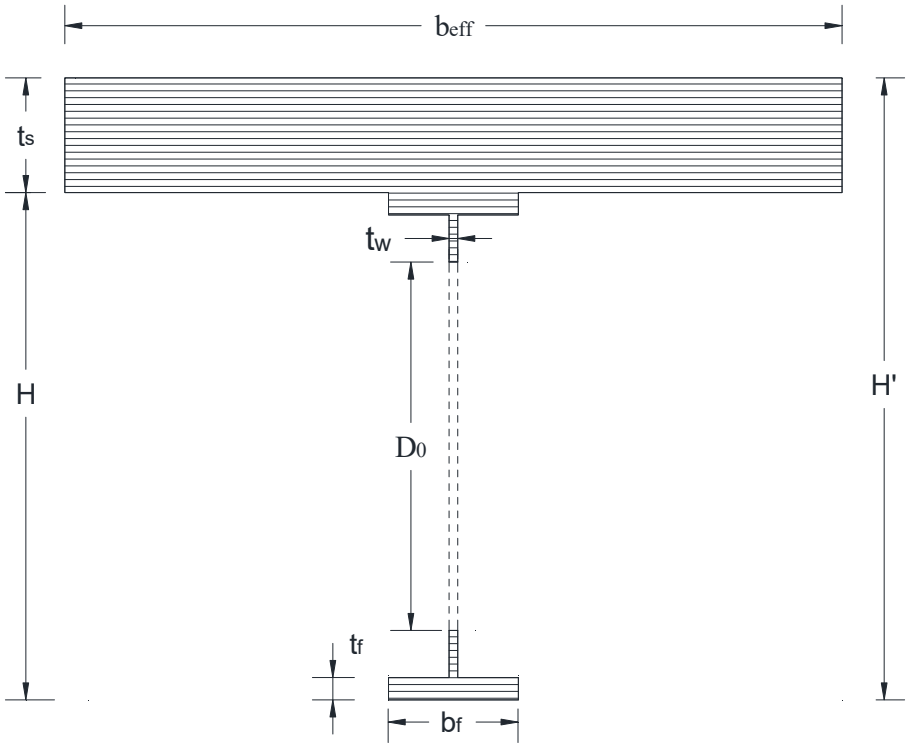

(b) CCS

Figure 1. Typical cross-section of composite beams.

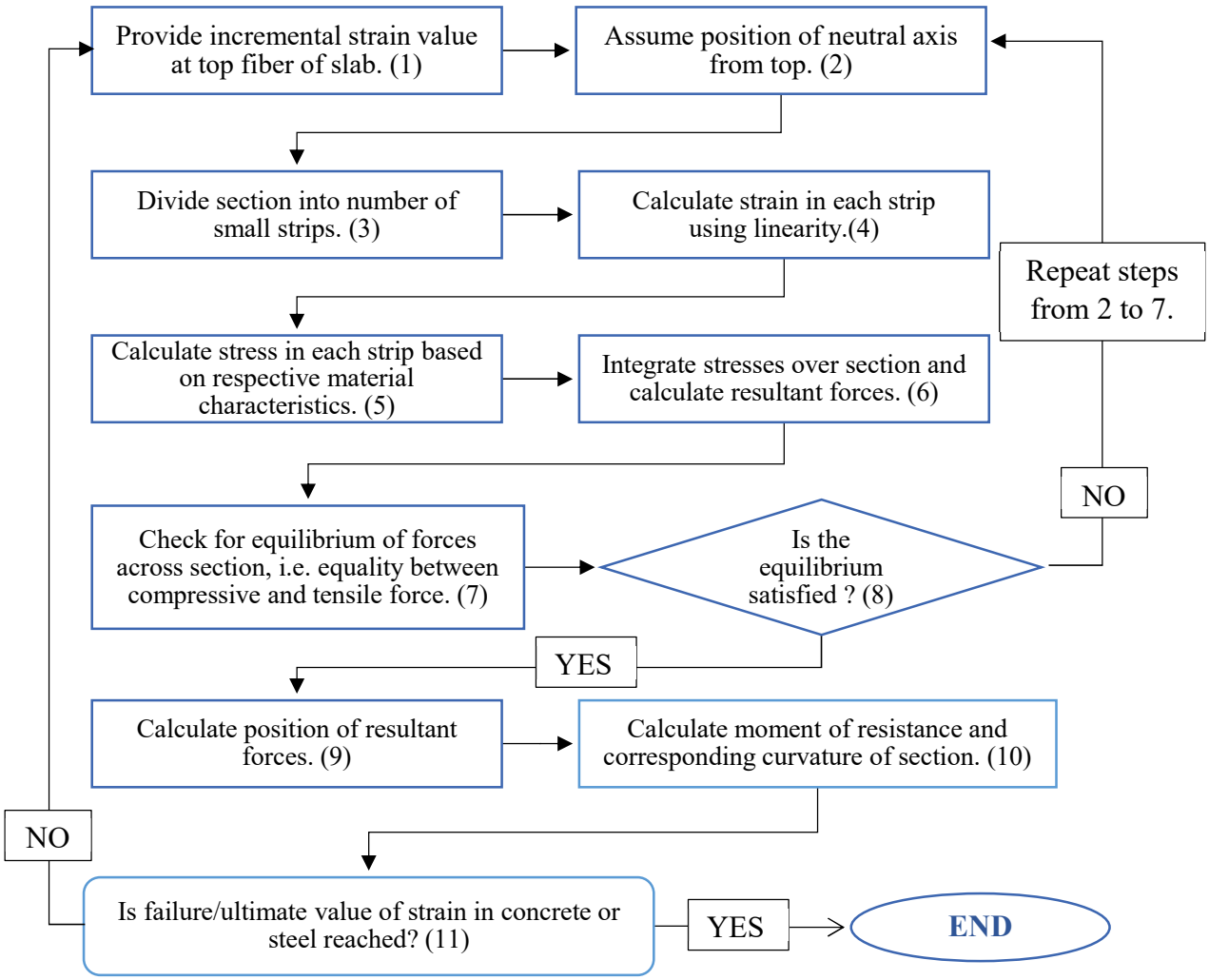

Figure 2: Flow-chart of a developed program for moment-curvature analysis.

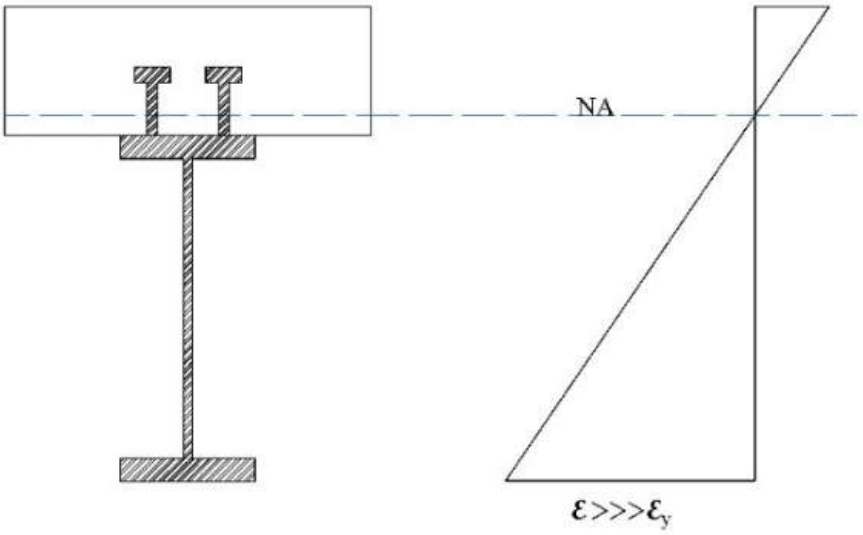

(a) SCS

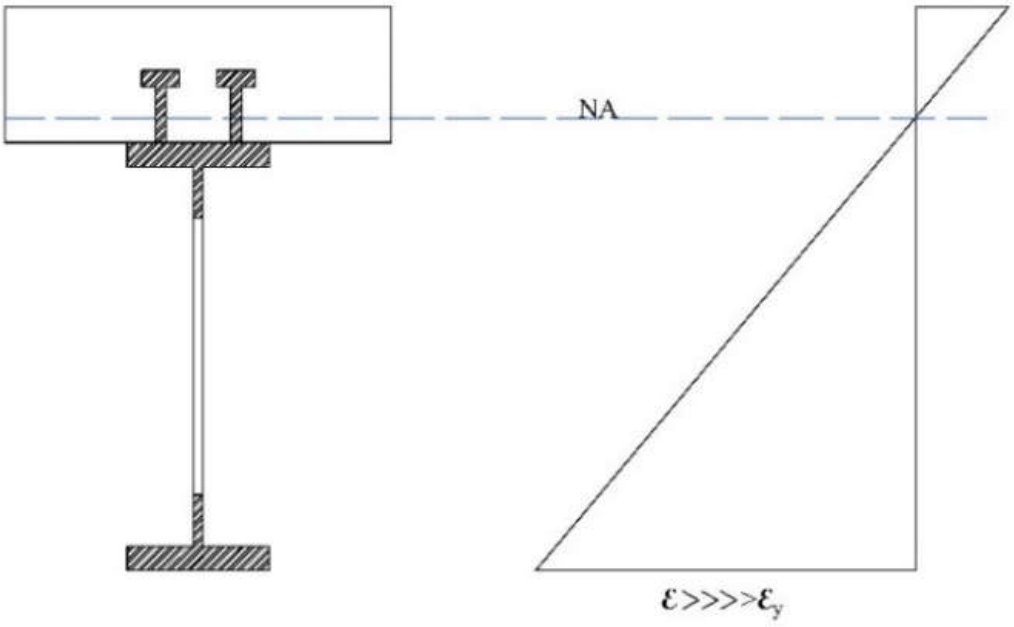

(b) CCS

Figure 3. Strain variation in composite cross-sections at the intermediate stage.

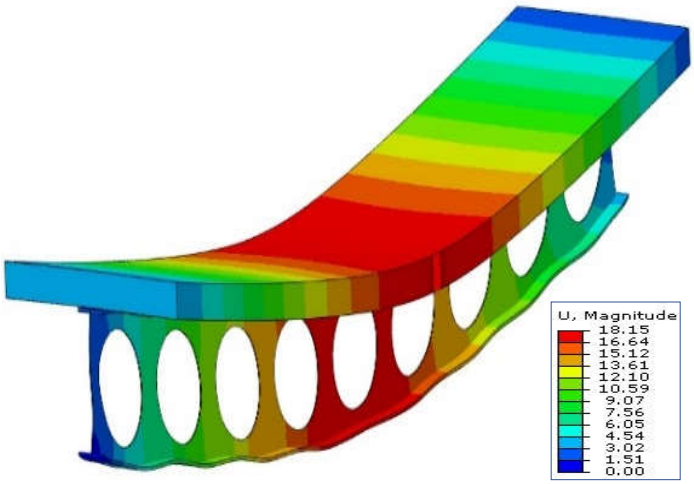

Figure 4. Present FE model of cellular composite beam.

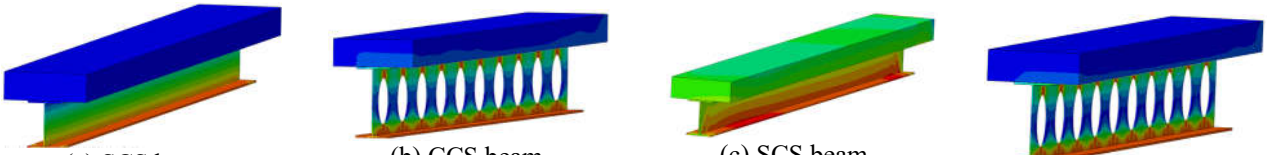

(a) SCS beam, unconfinement. (b) CCS beam, unconfinement. (c) SCS beam, confinement. (d) CCS beam, confinement

Figure 5. FE model of composite beams.

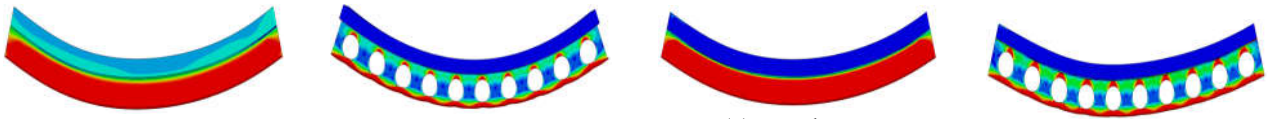

(a) SCS beam, unconfinement (b) CCS beam, unconfinement. (c) SCS beam, confinement. (d) CCS beam, confinement

Figure 6. Stress variation in composite beams.

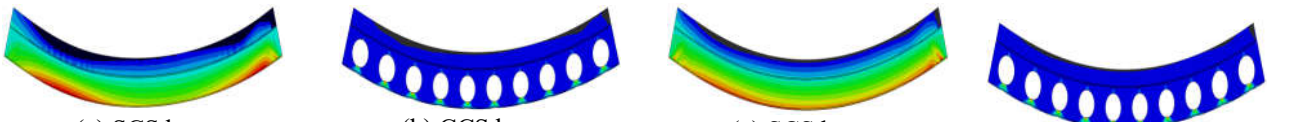

(a) SCS beam, unconfinement (b) CCS beam, unconfinement. (c) SCS beam, confinement. (d) CCS beam, confinement

Figure 7. Strain variation in composite beams.

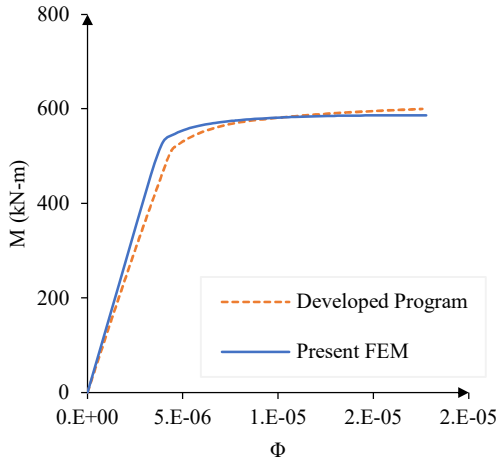

(a) SCS beam, unconfined

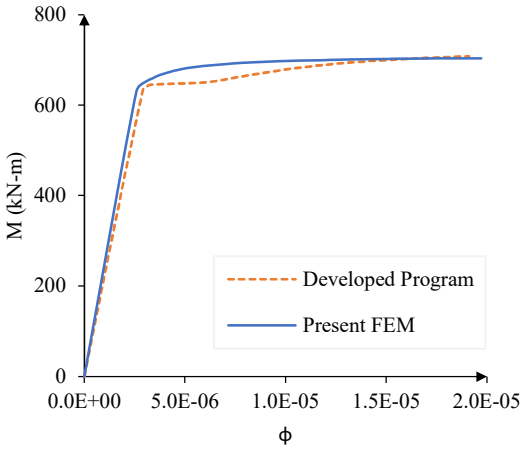

(b) CCS beam, unconfined

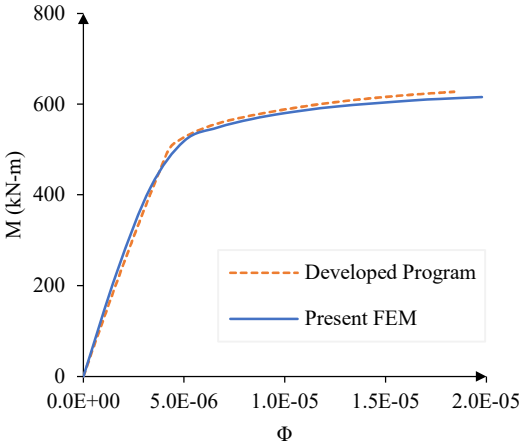

(c) SCS beam, confined

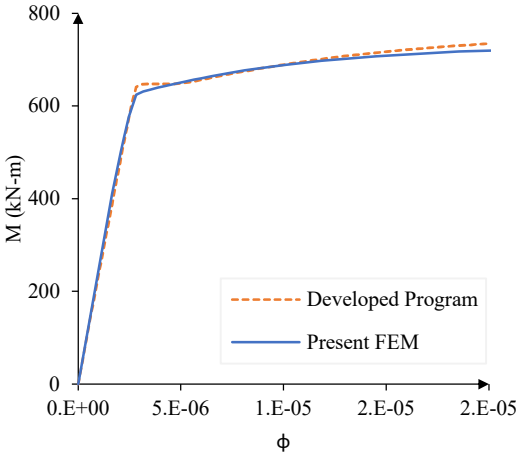

(d) CCS beam, confined

Figure 8. Moment-curvature behaviour of composite beams.

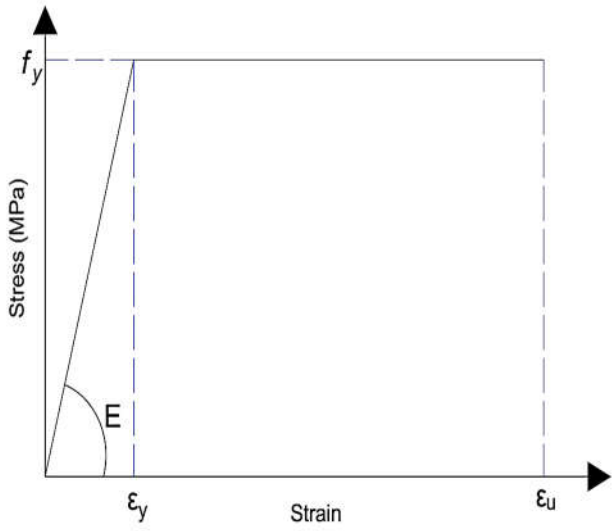

Figure 9. Bi-linear stress-strain curve of steel for both tension and compression.

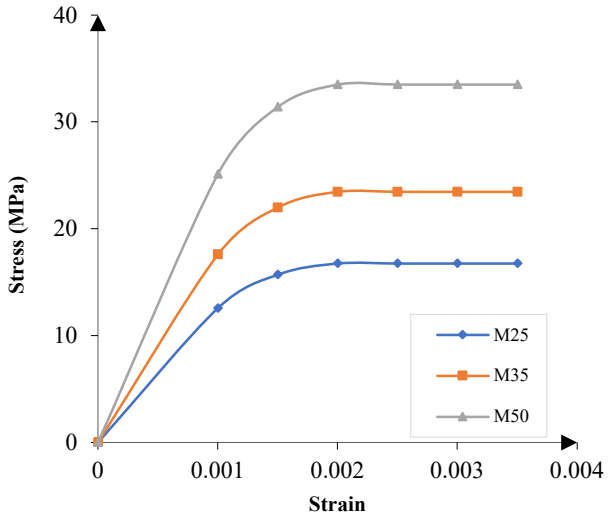

Figure 10. Idealized stress-strain curve of concrete in compression.

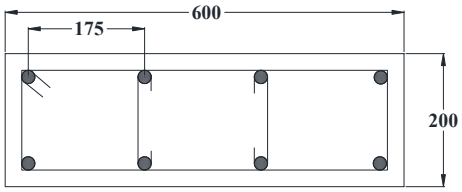

(a) b_{eff} = 600 mm

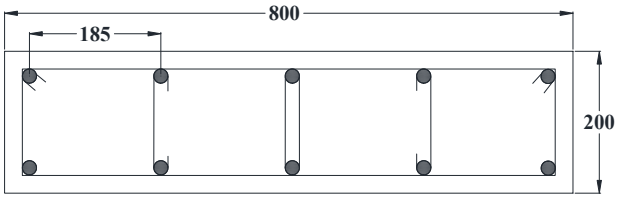

(b) b_{eff} = 800 mm

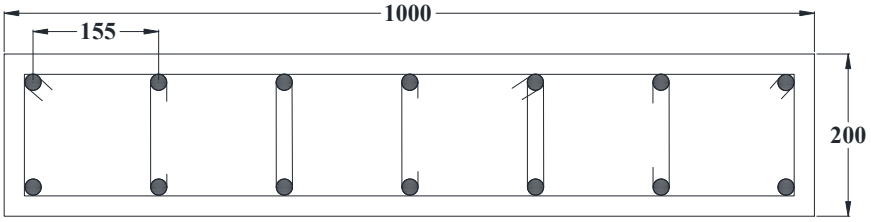

(c) b_{eff} = 1000 mm

Figure 11. Arrangement of reinforcement in concrete slab for a different $b_{eff.}$

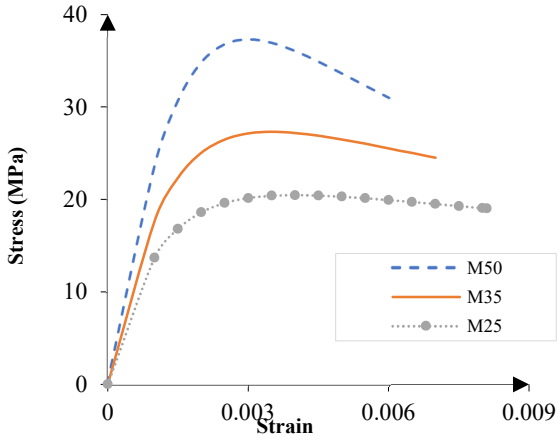

(a) b_{eff} = 600 mm

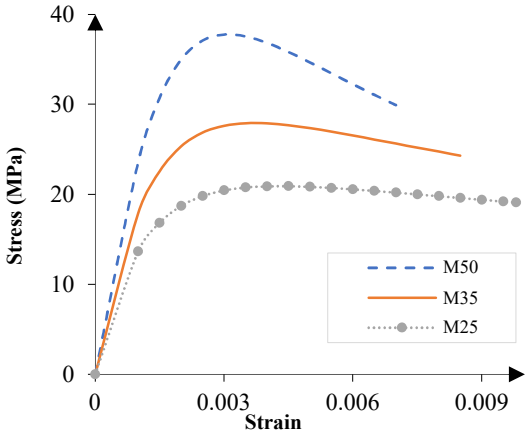

(b) b_{eff} = 800 mm

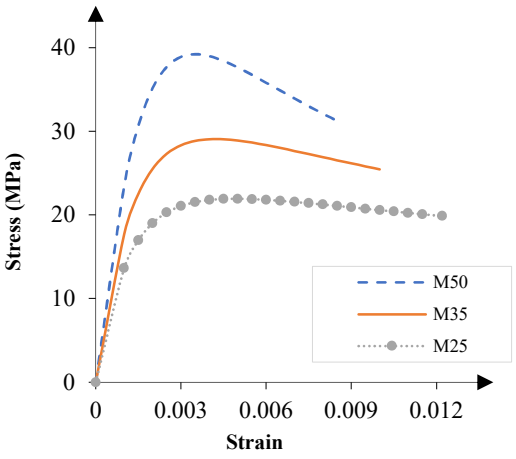

(c) b_{eff} = 1000 mm

Figure 12. Stress-strain curve for confined concrete.

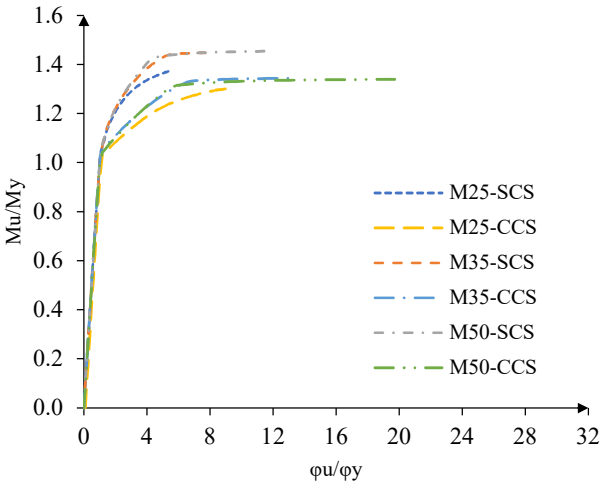

(a) Unconfined strength of concrete

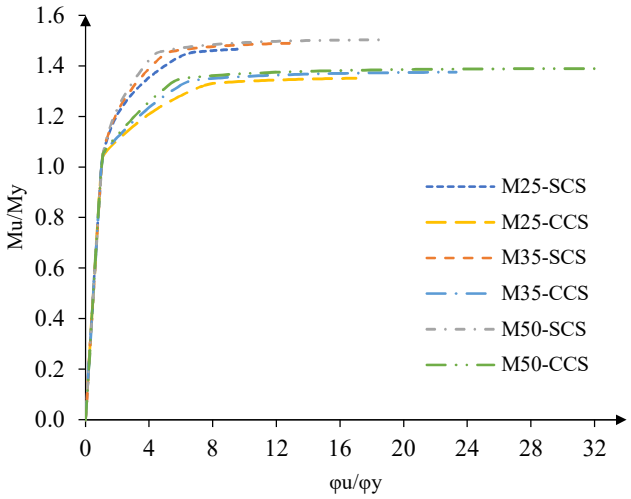

(b) Confined strength of concrete

Figure 13. Effect of the grade of concrete on composite sections.

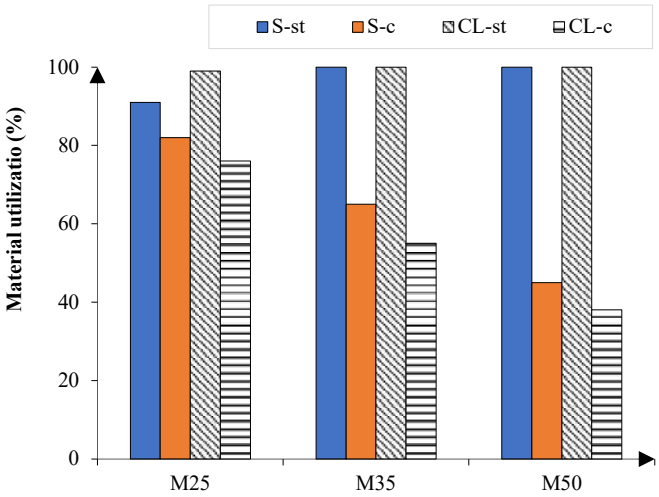

(a) Unconfined strength of concrete

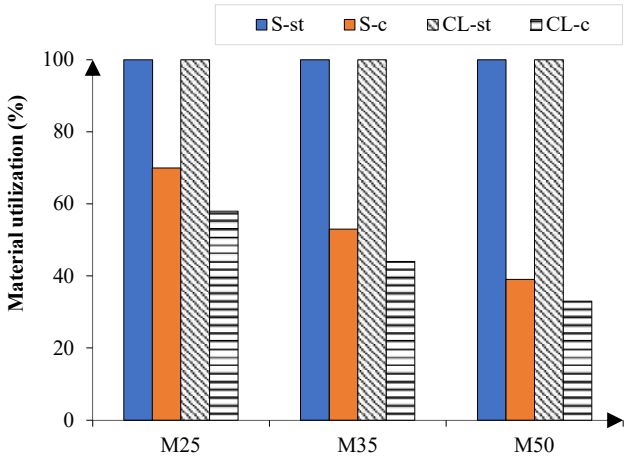

(b) Confined strength of concrete

Figure 14. Effect of different grades of concrete on material utilization of composite section having b_{eff} =1000 mm.

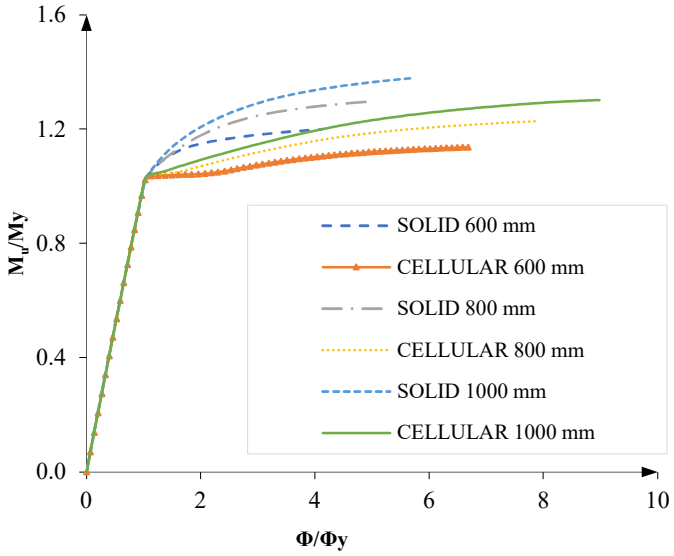

(a) Unconfined strength of concrete

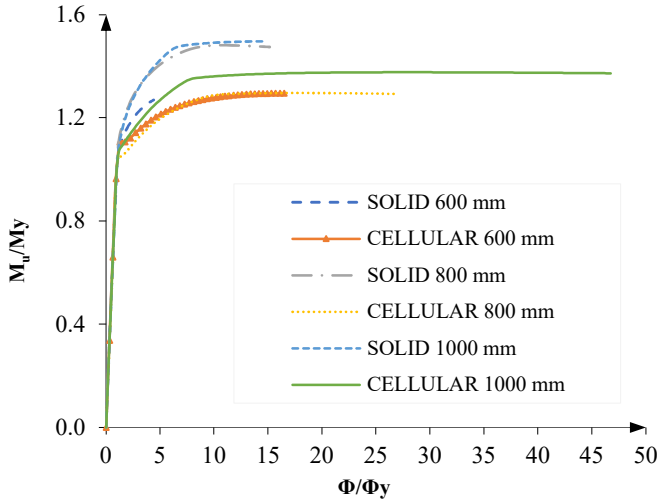

(b) Confined strength of concrete

Figure 15. Effect of effective flange width of slab on composite cross-sections.

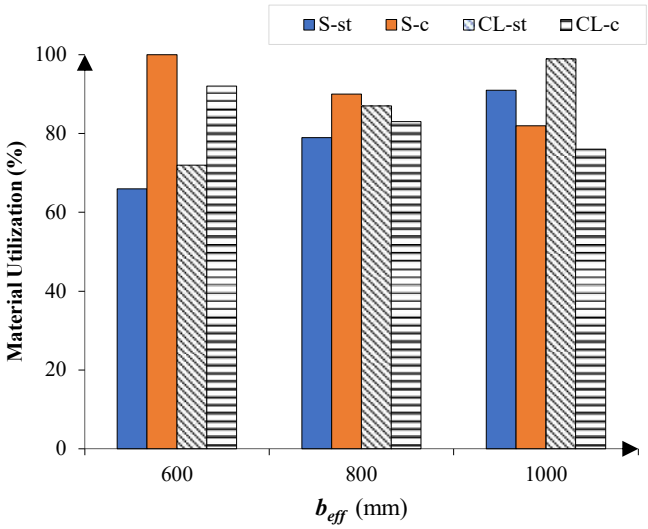

(a) Unconfined strength of concrete

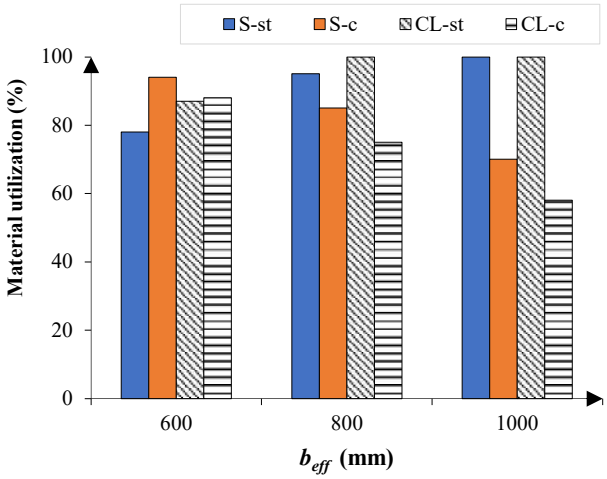

(b) Confined strength of concrete

Figure 16. Effect of different b_{eff} *on* material utilization of the cross-sections having M25 grade concrete.